Rock Stiffness and Permeability During Crack Opening And Closure: A Planar Transverse Isotropic (PTI) Model Using Pore Size Distributions (PSD)

C. Arson[1] and J.-M. Pereira[2]

[1]School of Civil and Environmental Engineering, Georgia Institute of Technology, 790 Atlantic Drive, Atlanta, GA30332-0355, USA; PH 404-385-0143; FAX 404-894-2278; email: chloe.arson@ce.gatech.edu
[2]Université Paris-Est, Laboratoire Navier (UMR 8205), CNRS – ENPC – IFSTTAR, F-77455 Marne-la-Vallée, France; email: jeanmichel.pereira@enpc.fr

ABSTRACT

A micro-macro model is proposed to study opening and closure of parallel crack planes in a porous rock. Pore Size Distributions (PSDs) of natural pores and cracks are updated with volumetric fractions, defined as distinct components of volumetric deformation. Deformation components depend on total deformation and on the crack density tensor (damage). The expression of the free energy postulated in the model allows capturing damage-induced anisotropy of stiffness. A unilateral condition of damage is introduced to account for stiffness recovery in compression. The permeability tensor is related to PSDs by combining Darcy's law and Hagen-Poiseuille flow equation. The model captures Planar Transverse Isotropy (PTI) induced by crack openings in both stiffness and permeability and predicts the evolution of two partial porosities (natural and damage-induced). The model will be used to model the damaged zone around underground cavities, faults and hydraulic fractures.

1 INTRODUCTION

Fault structure models usually assume that strain localizes in a core surrounded by a distribution of fractures forming a damage zone. Aligned crack arrays play an important role at several stages of faulting: microscopic tension does not change initial crack orientation, whereas microscopic shear stress opens predominant wing linkage cracks (thus rotating the principal direction of crack arrays). Crack damage decreases rock strength and induces stiffness anisotropy [6]. It is well known for instance that crack arrays parallel to the fracture plane have a shielding effect, whereas crack arrays perpendicular to the fracture plane tend to favor fracture propagation [11, 4]. The same fault displacements that originate stress concentrations at fracture tips can also close fractures present in the damaged zone - depending on the orientation of the pre-existing structure, and on the amount of confining pressure present in the bedrock [3, 12]. The model proposed in the following aims to determine the stiffness and permeability tensors of a solid, containing a uniform distribution of elastic pores and a

distribution of parallel crack planes. This configuration is known as Planar Transverse Isotropy (PTI). Anisotropic permeability models based on Continuum Damage Mechanics (CDM) generally assume that crack planes grow in directions perpendicular to the maximum principal (tensile) stress, and that accordingly, crack planes parallel to direction 1 mainly enhance permeability in direction 1 [10]. The self-consistent method allowed the prediction of percolation thresholds in rock containing an isotropic distribution of (spherical) defects of equal sizes [7]. In reality, the fabric tensor necessary to characterize damaged stiffness is different from the one necessary to predict permeability of a cracked medium [8]. Section 2 gives the model outline. Simulation of a uniaxial tension test including loading and unloading is explained in Section 3.

2 MODELING

The authors recently proposed a multi-scale isotropic permeability model for damaged rock [1, 9]. The underlying assumption is that natural pores and cracks can be considered as two separate sets of pores, characterized by two different size distributions ($p_p(r)$ and $p_c(r)$ respectively). The intrinsic permeability is obtained by combining Hagen-Poiseuille flow equation and Darcy's law [5]:

$$k_{int} = \frac{\Phi}{8 \int_0^\infty \left(N_p\, p_p(r) + N_c\, p_c(r)\right) \pi r^2 dr} \int_0^\infty \left(N_p\, p_p(r) + N_c\, p_c(r)\right) \pi r^4 dr \qquad (1)$$

in which N_p and N_c denote the number of natural pores and cracks in the Representative Elementary Volume, and Φ is total porosity (i.e. porosity due to both natural pores and cracks). Volumetric fractions of pores (V_p) and cracks (V_c) are related to the parameters of the bimodal Pore size Distribution ("PSD"):

$$V_p = \pi\, N_p \int_{r^p_{min}}^{r^p_{max}} p_p(r) r^2 dr \qquad\qquad V_c = \pi\, N_c \int_{r^c_{min}}^{r^c_{max}} p_c(r) r^2 dr \qquad (2)$$

The bounds of the integrals in Eq. 2 define the ranges of values that can be taken by natural pore and crack sizes. PSD curves are coupled to the mechanical behavior of the rock by updating microscopic parameters (e.g., average pore size) with deformation ($\boldsymbol{\epsilon}$) and damage ($\mathbf{D}$):

$$V_p = Tr\left(\boldsymbol{\epsilon}^{el}\right) \qquad\qquad V_c = Tr\left(\boldsymbol{\epsilon}^{d}\right) \qquad (3)$$

in which deformation is decomposed into: $\boldsymbol{\epsilon} = \boldsymbol{\epsilon}^{el} + \boldsymbol{\epsilon}^{ed} + \boldsymbol{\epsilon}^{id}$ where:

- $\boldsymbol{\epsilon}^{el}$ is the purely elastic strain
- $\boldsymbol{\epsilon}^{ed}$ is the additional elastic deformation induced by reduction of stiffness due to cracking
- $\boldsymbol{\epsilon}^{id}$ is the residual deformation induced by crack opening, which represents tensile strain remaining after relaxation of tension stress. $\boldsymbol{\epsilon}^{id}$ depends on the expression of the free energy.

In the following, total elastic deformation is noted $\boldsymbol{\epsilon}^E = \boldsymbol{\epsilon}^{el} + \boldsymbol{\epsilon}^{ed}$. The main constitutive equations employed in this study are summarized in Tab. 1. The damage variable (noted $\mathbf{D}$) is defined as the second-order crack density tensor. Its work-conjugate variable (noted $\mathbf{Y}$) is split in order to separate the energy release rate responsible for stiffness weakening and the energy release rate associated with residual crack opening. It is assumed that only the positive part of the latter (noted $\mathbf{Y_1^+}$) drives crack propagation.

Table 1. Main Equations of the Constitutive Model.

Functional	Postulated Expression
Free Energy (Ψ_s)	$\Psi_s\left(\boldsymbol{\epsilon}^E, \mathbf{D}\right) = \frac{1}{2}\boldsymbol{\epsilon}^E : \mathbf{C}(\mathbf{D}) : \boldsymbol{\epsilon}^E - g\mathbf{D} : \boldsymbol{\epsilon}$
Damage Function (f_d)	$f_d\left(\mathbf{Y_1^+}, \mathbf{D}\right) = \sqrt{\frac{1}{2}\mathbf{Y_1^+} : \mathbf{Y_1^+}} - C_0 - C_1 Tr\left(\mathbf{D}\right)$, with $\mathbf{Y_1^+} = -g\epsilon^+$
Deformation Component	**Incremental Expression**
Pure Elastic ($\boldsymbol{\epsilon}^{el}$)	$d\boldsymbol{\epsilon}^{el} = {\mathbf{C_0}}^{-1} : d\boldsymbol{\sigma}$
Elastic Damaged ($\boldsymbol{\epsilon}^{ed}$)	$d\boldsymbol{\epsilon}^{ed} = \left[\mathbf{C}(\mathbf{D})^{-1} - {\mathbf{C_0}}^{-1}\right] : d\boldsymbol{\sigma}$
Irreversible Damaged ($\boldsymbol{\epsilon}^{id}$)	$d\boldsymbol{\epsilon}^{id} = \mathbf{C}(\mathbf{D})^{-1} : (-g) d\mathbf{D}$

In this paper, the model is extended to unilateral effects induced by crack closure on stiffness and permeability. As a first step, the study is restricted to Planar Transverse Isotropy (PTI) - when all cracks in the sample are contained in parallel planes. In the proposed orthotropic damage model, PTI is encountered in uniaxial tension tests. For instance tensile strain in direction 1 (ϵ_1^+) opens cracks contained in planes normal to direction 1, which can potentially close due to compressive strain in direction 1 (ϵ_1^-) - as illustrated in Fig 1. Crack closure induces a decrease of elastic damaged deformation ($\boldsymbol{\epsilon}^{ed}$), and therefore, a reduction of crack volume (V_c) and permeability. In addition, compressive strength in direction 1 is recovered (while tensile strength is not). Constitutive equations are not significantly changed: a unilateral condition is introduced in the expression of damaged rock stiffness tensor:

$$\widetilde{\mathbf{C}}(\mathbf{D}) = \mathbf{C}(\mathbf{D}) + \sum_{k=1}^{3} H(-\epsilon^{(k)}) \left[\mathbf{C_0} - \mathbf{C}(\mathbf{D})\right] \tag{4}$$

in which $\epsilon^{(k)}$ is the $k-th$ eigenvalue of the deformation tensor.

Let's consider the cross-section (in plane (x_2, x_3)) of a rock sample subjected to pure tension in direction 1. Degradation of stiffness induced by damage corresponds to a decrease of material surface within the cross-section that can *effectively* resist the tensile load applied in direction 1, i.e. a decrease of *effective* cross-section area. In one

dimension, *effective stress* is the ratio of internal normal forces by effective cross-section area, which provides a direct relationship between actual stress, effective stress and damage. In a three-dimensional analysis, damage is a tensor variable, often defined as the second-order crack density tensor. The relationship between actual and effective stress requires the definition of a tensor damage operator. In the following simulations, the undamaged material is linear elastic (with a Young's modulus E_0 and a Poisson's ratio ν_0), and the damaged stiffness tensor is obtained by applying the Principle of Equivalent Elastic Energy (which states that the elastic strain energy stored by a damaged sample subjected to the actual stress is equal to the elastic strain energy stored by an undamaged sample subjected to effective stress) with the damage operator of Cordebois and Sidoroff (which ensures positivity and symmetry requirements). For a PTI case damage eigenvalues in directions 2 and 3 are equal to zero: $d_2 = d_3 = 0$. The expression of the stiffness tensor is obtained by introducing the unilateral condition (equation 4) in the stiffness expression (explained in [2]). Using Voigt notations:

$$\widetilde{\mathbf{C}}\left(\mathbf{D}\right) = \frac{E_0}{(1-2\nu_0)(1+\nu_0)} \times$$

$$\begin{bmatrix} (1-\nu_0)\widetilde{C}_1(d_1,\epsilon_1) & \nu_0\widetilde{C}_2(d_1,\epsilon_1) & \nu_0\widetilde{C}_2(d_1,\epsilon_1) & & & & \\ \nu_0\widetilde{C}_2(d_1,\epsilon_1) & (1-\nu_0) & \nu_0 & & & & \\ \nu_0\widetilde{C}_2(d_1,\epsilon_1) & \nu_0 & (1-\nu_0) & & & & \\ 0 & 0 & 0 & & & & \\ 0 & 0 & 0 & & & & \\ 0 & 0 & 0 & & & & \\ & & & (1-2\nu_0) & & & \\ & & & & (1-2\nu_0)\widetilde{C}_2(d_1,\epsilon_1) & & \\ & & & & & (1-2\nu_0)C_2(d_1,\epsilon_1) & \end{bmatrix} \tag{5}$$

in which:

$$\begin{aligned} \widetilde{C}_1(d_1,\epsilon_1) &= [H(-\epsilon_1) + (1-H(-\epsilon_1))(1-d_1)^2] \\ \widetilde{C}_2(d_1,\epsilon_1) &= [H(-\epsilon_1) + (1-H(-\epsilon_1))(1-d_1)] \end{aligned} \tag{6}$$

In which $H(.)$ denotes Heaviside function. The damaged permeability model assumes that cracks do not intersect but that they are connected to the porous network made of "natural pores" (i.e., the pores existing prior to loading). The model proposed by the authors in [1] was restricted to open cracks having a uniform orientation distribution. In the present study, cracks are alined, and can be either open or closed. In this PTI configuration, the fluid cannot flow from one horizontal crack (perpendicular to direction 1) to the other through an intersecting crack in a plane parallel to the axis (because

there is no vertical crack). As a result, damage-induced preferential flow paths are expected to localize in (horizontal) crack planes. It is proposed to model the resulting anisotropic permeability tensor as follows:

$$\mathbf{K}(\mathbf{D}) = \begin{bmatrix} k_p & 0 & 0 \\ 0 & k_{p,c} & 0 \\ 0 & 0 & k_{p,c} \end{bmatrix} \tag{7}$$

in which:

$$\begin{aligned} k_p &= \frac{\Phi}{8\int_0^\infty N_p\, p_p(r)\, \pi r^2 dr} \int_0^\infty N_p\, p_p(r)\, \pi r^4 dr \\ k_{p,c} &= \frac{\Phi}{8\int_0^\infty (N_p\, p_p(r) + N_c\, p_c(r))\pi r^2 dr} \int_0^\infty (N_p\, p_p(r) + N_c\, p_c(r))\, \pi r^4 dr \end{aligned} \tag{8}$$

Permeability variations induced by crack closure automatically result from the unilateral condition above, due to the relationship between permeability and deformation (this will be illustrated in the simulation presented next).

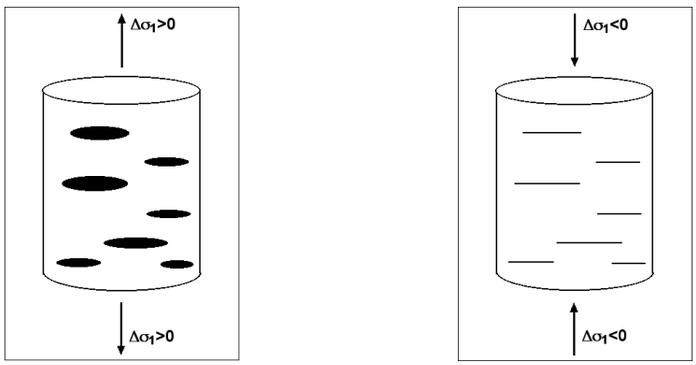

Figure 1. Planar Transverse Isotropy induced by crack-opening (left) and closure (right).

3 SIMULATION OF A UNIAXIAL TENSION TEST

3.1 Computational Algorithm

The theoretical loading/unloading path expected for a uniaxial tension test in $\sigma_1 - \epsilon_1$ space is sketched in Fig. 2. The tension loading phase stands in the elastic domain first (OA), and then in the damaged domain (AB). This is followed by a compression phase. During crack closure, the stress/strain diagram follows a linear unloading path (BC & CD), exhibiting a damaged rigidity (i.e. the slope of BC&CD is less than the slope of OA). As soon as deformation becomes compressive ($\epsilon_1 < 0$, DE), stiffness is recovered by crack closure (unilateral effects). Three cases can occur:

- Under compressive deformation ($\epsilon_1 < 0$, case DE), the response is elastic (assuming that the test is controlled so as to remain below the compression damage limit). In addition, unilateral effects impose that stiffness in compression should be equal to the reference (undamaged) stiffness.

- Under tensile deformation ($\epsilon_1 > 0$) and compressive loading ($\Delta\epsilon_1 < 0$, cases BC, CD), the response is elastic (assuming that the test is controlled so as to remain below the compression damage limit). During this unloading path, stiffness is damaged (with zero damage if the sample is unloaded before crack opening at A).

- Under tensile deformation ($\epsilon_1 > 0$) and tensile loading ($\Delta\epsilon_1 > 0$), the response is elastic below the tension limit (case OA). The loading path stands in the damaged domain above this limit (case AB).

The constitutive relationships that need to be updated in the course of the algorithm are summarized in Tab. 2.

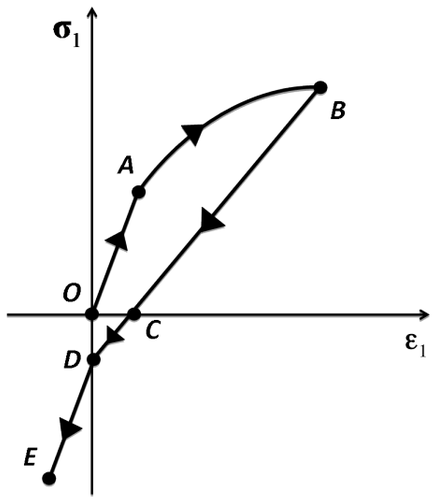

Figure 2. Theoretical Loading/Unloading Path During a Uniaxial Tension Test.

3.2 Physical Test Simulated

A strain-controlled uniaxial tension test is simulated in order to study model predictions of rock stiffness and permeability of rock in a damage-induced PTI configuration. Unloading in compression is controlled so as to ensure that the load path remains in the elastic domain. Tension is applied in direction 1 ($\Delta\epsilon_1 = 3.5 \cdot 10^{-3}$; $\Delta\sigma_2 = \Delta\sigma_3 = 0$). Tension loading is followed by a compression phase, so as to compensate axial strain developed in tension ($\Delta\epsilon_1 = -3.5 \cdot 10^{-3}$; $\Delta\sigma_2 = \Delta\sigma_3 = 0$). Material parameters chosen for this numerical study are typical of a granite (Tab. 3).

Table 2. Principle of the Algorithm.

Loading Case	Macroscopic Relationships	Crack Volume
$\epsilon_1 < 0$ (DE)	$\Delta\sigma = \mathbf{C_0} : \Delta\epsilon^{el}$, $\Delta\epsilon = \Delta\epsilon^{el}$	$\Delta V_c = 0$, $V_c = 0$
$\epsilon_1 > 0$, $\Delta\epsilon_1 < 0$ (BC, CD)	$\Delta\mathbf{D} = 0$, $\Delta\epsilon^{id} = 0$ $\Delta\sigma = [\mathbf{C}(\mathbf{D}) - \mathbf{C_0}] : \Delta\epsilon^{ed}$	$\Delta V_c = Tr(\Delta\epsilon^{ed})$
$\epsilon_1 > 0$, $\Delta\epsilon_1 > 0$ elastic (OA)	$\Delta\mathbf{D} = 0$, $\Delta\epsilon^{id} = 0$ $\Delta\sigma = [\mathbf{C}(\mathbf{D}) - \mathbf{C_0}] : \Delta\epsilon^{ed}$ initially: $\mathbf{D} = 0$	$\Delta V_c = Tr(\Delta\epsilon^{ed})$
$\epsilon_1 > 0$, $\Delta\epsilon_1 > 0$ damage (BC)	$\Delta\mathbf{D} \neq 0$ $-g\Delta\mathbf{D} = \mathbf{C}(\mathbf{D}) : \Delta\epsilon^{id}$ $\Delta\sigma = [\mathbf{C}(\mathbf{D}) - \mathbf{C_0}] : \Delta\epsilon^{ed}$	$\Delta V_c = Tr(\Delta\epsilon^{ed} + \Delta\epsilon^{id})$

Table 3. Material Parameters Used in the Simulations.

Ref. Young's Modulus	Ref. Poisson's Ratio	"Toughness" Parameter	Init. Damage Threshold	Damage Rate Parameter
E_0 (MPa)	ν_0 (-)	g (MPa)	C_0 (MPa)	C_1 (MPa)
8,010	0.28	-330	0.11	2.2
Min. Pore Radius	Max. Pore Radius	Min. Crack Size	Max. Crack Size	Init. Void Ratio
r^p_{min} (μm)	r^p_{max} (μm)	r^c_{min} (μm)	r^c_{max} (μm)	e_0 (-)
0.01	1	1	10	0.015

3.3 Results

The stress/strain diagram in Fig. 3.a illustrates the theoretical features of segments (OA-AB-BC-CD) in the sketch of Fig. 2. As expected, cracks develop only in planes perpendicular to the loading axis, i.e. $D_2 = D_3 = 0$, $D_1 \neq 0$. There is no crack propagation during compressive unloading (i.e. $\Delta\mathbf{D} = 0$), as noted from the vertical line at $D_1 = 0.32$ in Fig. 3.b. Permeability in the direction of loading (k_p) stays almost constant with a sligth increase during tension and slight decrease during unloading (Fig. 4.a& b.). Permeability in the lateral directions ($k_{p,c}$) increases by one order of magnitude during crack propagation in tension (Fig. 4.b.). Compression unloading closes cracks within the elastic damaged deformation domain. Residual crack openings contribute to most damage-induced permeability, as can be noted by the value of $k_{p,c}$ at the end of the test (Fig. 4.a.).

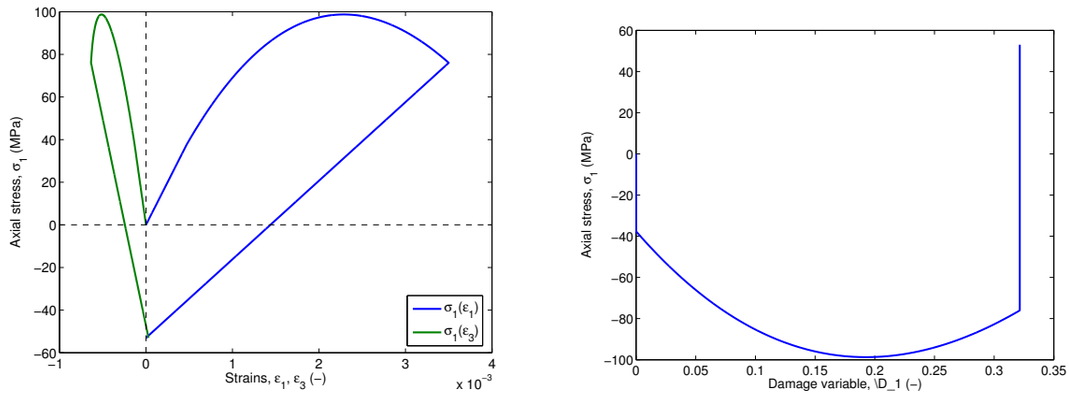

(a) (b)

Figure 3. Mechanical Loading Path Simulated: (a) Stress/Strain Diagram. (b) Evolution of Damage.

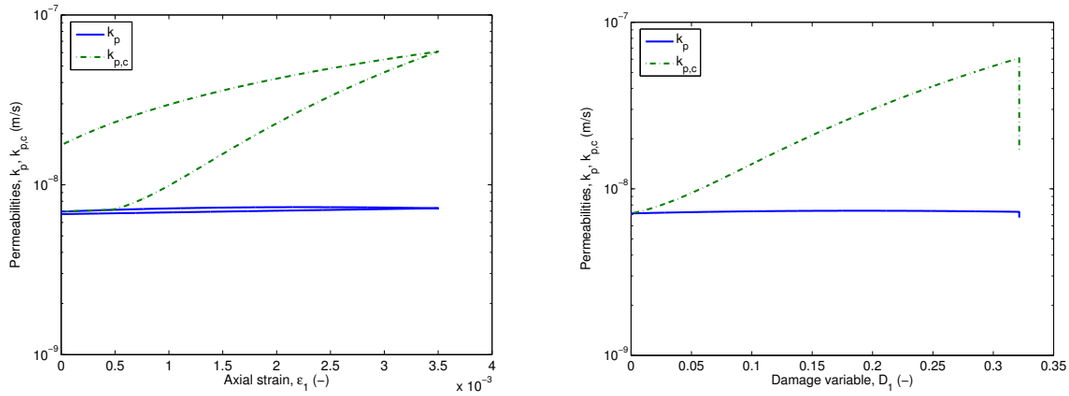

(a) (b)

Figure 4. Components of the Permeability Tensor: (a) Versus Axial Strain (b) Versus Lateral Damage.

Fig. 5.a. indicates that cracks appear for $\epsilon_1 \approx 0.5 \cdot 10^{-3}$. An increase of crack volumetric fraction (V_c) follows during the tension loading phase. The volume of cracks decreases linearly with compressive deformation upon unloading (damaged elastic load path BC& CD in Fig. 2). The volumetric fraction of natural pores V_p (contributing to purely elastic deformation only) sightly increases at the beginning the tension loading phase but starts to decrease after the axial stress peak. During the unloading stage, V_p continues to slightly decrease because of the reduction of the mean stress. The Pore Size Distribution assumed before loading reflects the choice of a normal size distribution for natural pores (Fig. 5.b). In tension, the elastic limit is reached for low values of deformation: crack-induced irreversible deformation is low compared to elastic deformation. This explains why it is difficult to see the occurrence of a second porosity mode associated to the cracks in Fig. 5.b. Cracks opening in tension form a set of large

pores, which decreases the partial porosity of natural pores. After unloading, porosity associated to both natural pores and cracks decrease slightly but do not recover their initial values. The decrease of V_p is compensated by the presence of cracks that do not close so that the REV volume (reflected by V_v, see Fig. 5.a) at the end of the loading-unloading cycle almost recovers its initial value. This is in agreement with the almost superposed cumulative porosity curves for initial and unloaded states in Fig. 5.b.

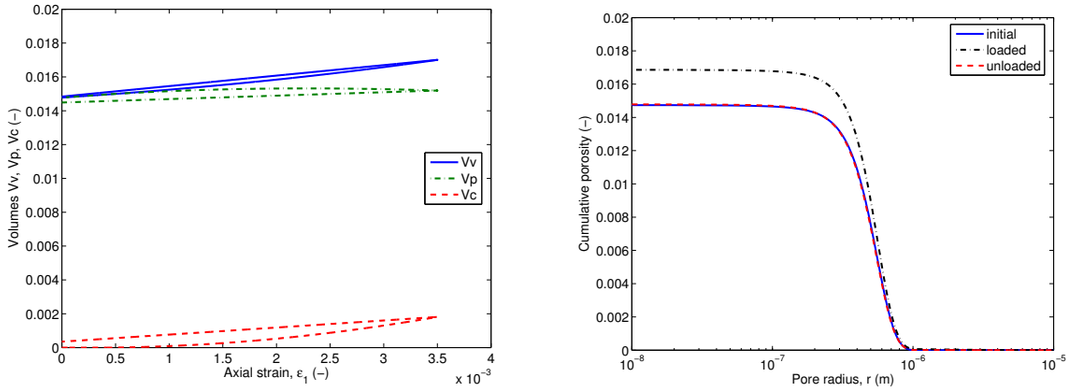

(a) (b)

Figure 5. Microstructure changes: (a) Evolution of pore volumes in the REV. (b) Evolution of the Cumulative PSDs.

4 CONCLUSION

A micro-macro model based on Continuum Damage Mechanics (CDM) is proposed to study opening and closure of parallel crack planes in a porous rock. Damage is defined as a second-order tensor, under the assumptions that cracks are not connected one to another, but that they are connected to the natural porous network (in a reference state before crack propagation). Statistical parameters of the Pore Size Distributions (PSDs) of natural pores and cracks are updated with volumetric fractions, which are defined as distinct components of volumetric deformation. These components are computed from damage and total deformation. The expression of the free energy postulated in the model allows capturing damage-induced anisotropy of stiffness. A unilateral condition of damage is introduced in order to account for the recovery of stiffness in compression. The permeability tensor is related to PSDs by combining Darcy’s law and Hagen-Poiseuille flow equation. Because of the Planar Transverse Isotropy (PTI) induced by crack openings, enhancement of permeability is expected in the directions perpendicular to the loading axis only. The model captures these anisotropic effects on both the stiffness tensor and the permeability tensor. At the microscopic level, the model also predicts the evolution of the two partial porosities (natural and damage-induced). Further developments will be dedicated to permeability variations in the compression domain after unloading (DE in Fig. 2), to further relate damaged stiffness and permeability to the evolution of fully anisotropic crack distributions - open compression

cracks adding to closed tension cracks in particular. The model will be used to model the damaged zone around underground cavities, faults and hydraulic fractures.

REFERENCES

C. Arson, J.-M. Pereira: Influence of Damage on Pore Size Distribution and Permeability of Rocks, *International Journal for Numerical and Analytical Methods in Geomechanics*, DOI:10.1002/nag.1123

Chaboche, J. L. (1993). "Development of continuum damage mechanics for elastic solids sustaining anisotropic and unilateral damage." *International Journal of Damage Mechanics*, 2(4), 311-329.

Cowie, P.A., 1998. A healing-reloading feedback control on the growth rate of seismogenic faults. Journal of Structural Geology 20, 8, 1075-1087.

Fu, P., Johnson, S.M., Carrigan, C., 2012. An explicitly coupled hydro-geomechanical model for simulating hydraulic fracturing in complex discrete fracture networks. International Journal for Numerical and Analytical Methods in Geomechanics, DOI: 10.1002/nag.2135

I. Garcia-Bengoechea, C. Lowell, A. Altschae, Pore distribution and permeability of silty clays, *J. Geotech. Eng. Div.* 105 (1979) 839-856.

Ibanez, W.D, Kronenberg, A.K., 1993. Experimental Deformation of Shale: Mechanical Properties and Micrstructural Indicators of MEchanisms. Int. J. Rock Mech. Min. Sci. & Geomech. Abstr. 30, 7, 723-734.

D. Kondo, L. Dormieux, Approche micro-mécanique du couplage per- mabilité- endommagement, *Comptes-Rendus de Mécanique*, Acad. Sci. Paris 332 (2004) 135-140.

K. Maleki, A. Pouya, Numerical simulation of damage-Permeability relationship in brittle geomaterials, *Computers and Geotechnics* 37 (5) (2010) 619-628.

J. M. Pereira, C. Arson, Retention and permeability properties of damaged porous rocks, *Computers and Geotechnics* 48 (2013) 272-282.

J. Shao, H. Zhou, K. Chau, Coupling between anisotropic damage and permeability variation in brittle rocks, *International Journal for Numer- ical and Analytical Methods in Geomechanics* 29 (2005) 1231-1247.

Wu, S., Chudnovsky, A., 1993. Effect of microcrack array on stress intensity factor of main crack. International Journal of Fracture 59, 41-52.

Zhang, X., Jeffrey, R.G., Thiercelin, M., 2007. Deflection and propagation of fluid-driven fractures at frictional bedding interfaces: A numerical investigation. Journal of Structural Geology 29, 396-410.